Quasi-elastic helium-atom scattering from surfaces: experiment and interpretation

2002 J. Phys.: Condens. Matter 14 6173

(http://iopscience.iop.org/0953-8984/14/24/315)

INSTITUTE OF PHYSICS PUBLISHING JOURNAL OF PHYSICS: CONDENSED MATTER

J. Phys.: Condens. Matter **14** (2002) 6173–6191 PII: S0953-8984(02)36386-0

Quasi-elastic helium-atom scattering from surfaces: experiment and interpretation

A P Jardine, J Ellis and W Allison

Cavendish Laboratory, Madingley Road, Cambridge CB3 0HE, UK

E-mail: apj24@cam.ac.uk

Received 30 April 2002
Published 31 May 2002
Online at stacks.iop.org/JPhysCM/14/6173

Abstract

Diffusion of an adsorbate is affected both by the adiabatic potential energy surface in which the adsorbate moves and by the rate of thermal coupling between the adsorbate and substrate. In principle both factors are amenable to investigation through quasi-elastic broadening in the energy spread of a probing beam of helium atoms. This review provides a topical summary of both the quasi-elastic helium-atom scattering technique and the available data in relation to the determination of diffusion parameters. In particular, we discuss the activation barriers deduced from experiment and their relation to the adiabatic potential and the central role played by the friction parameter, using the CO/Cu(001) system as a case study. The main issues to emerge are the need for detailed molecular dynamics simulations in the interpretation of data and the desirability of significantly greater energy resolution in the experiments themselves.

Contents

0953-8984/02/246173+19$30.00

1. Introduction

Surface diffusion is one of the most basic and important of dynamical processes. For example, the lateral motion of an adsorbed molecule can determine the outcome of a surface reaction or, in the case of growth, the motion of deposited atoms can give rise to kinetic effects that dominate the development of the surface morphology. Few techniques allow adsorbate motion to be explored directly and most of our current knowledge relies on inferences from kinetic measurements [1]. One experiment that gives direct insight into adsorbate dynamics is that of quasi-elastic helium-atom scattering (QHAS). As adsorbed particles move on the surface they create a dynamical target for a probe of helium atoms. The probe atoms experience small changes in velocity as they scatter from the moving target. These small changes manifest themselves as a broadening in the spread of energies around the elastic peak, usually referred to as the 'quasi-elastic' broadening. The quasi-elastic broadening is characteristic of the diffusion process and so, by making precise measurements of the elastic peak energy profile, QHAS analysis can be used to extract the underlying diffusional information.

Helium-atom scattering (HAS) has become a well established technique for studying both the structure and dynamics of surfaces [2–4]. The construction of very high-resolution inelastic scattering equipment, based on the time-of-flight method, has led to the development of the modern QHAS technique and its application to the study of surface diffusion [5, 6]. New methods are also under development. In particular, the spin-echo technique offers improvements in resolution by as much as four orders of magnitude [7]. In this article we review the principles of the QHAS experiment (including both time-of-flight and spin-echo energy measurements) and consider the methods for experimental analysis that have been developed. We also summarize the systems studied to date and illustrate the application of the principles by considering our recent results for the CO/Cu(001) system.

QHAS is the surface analogue of the well developed quasi-elastic neutron scattering technique, used to probe diffusion in bulk materials. In order to quantify the technique, the original theories for quasi-elastic neutron scattering [8–10] have been reapplied to the case of neutral-atom scattering from a two-dimensional surface. The foundations are based on representing diffusion using the Van Hove correlation function, $G(\boldsymbol{R}, t)$. Van Hove [8] showed that, in the single-scattering approximation, the differential scattering cross-section from a time-varying distribution of scatterers could be written as the Fourier transform, in space and time, of a suitable time-dependent pair correlation function. In terms of a differential reflection probability for helium atoms, $\partial^2 R/\partial\Omega\,\partial\omega$, the probability of scattering atoms into a given energy ($\partial\omega$) and solid angle ($\partial\Omega$) may be written as [11, 12]

$$\frac{\partial^2 R}{\partial\Omega\,\partial\omega}(\Delta\boldsymbol{K},\omega) = n_d|F(\Delta\boldsymbol{K},\omega)|^2 \iint G(\boldsymbol{R},t)\exp[\mathrm{i}(\Delta\boldsymbol{K}\cdot\boldsymbol{R}-\omega t)]\,\mathrm{d}\boldsymbol{R}\,\mathrm{d}t$$
$$= n_d|F(\Delta\boldsymbol{K},\omega)|^2 S(\Delta\boldsymbol{K},\omega). \tag{1}$$

where n_d is the density of scattering centres/particles on the surface, $F(\Delta\boldsymbol{K}, \omega)$ is the amplitude form factor for the scattering, due to the interaction of the helium with an individual scatterer, and $\Delta\boldsymbol{K}$ is the surface-projected momentum transfer on scattering. $S(\Delta\boldsymbol{K}, \omega)$ is the (intensity) dynamical structure factor, which represents the interaction of the helium with the time-varying ensemble of scatterers spread over the surface. The correlation function, $G(\boldsymbol{R}, t)$, represents the probability of finding a particle at position $\boldsymbol{R}$ at time t, given that there was a particle at position $\boldsymbol{R} = 0$ at time $t = 0$. In many cases, the form factor, $F(\Delta\boldsymbol{K}, \omega)$, varies slowly with $\Delta\boldsymbol{K}$ [5], so the shape of the energy-resolved quasi-elastic peak is simply given by $S(\Delta\boldsymbol{K}, \omega)$, the Fourier transform of the correlation function.

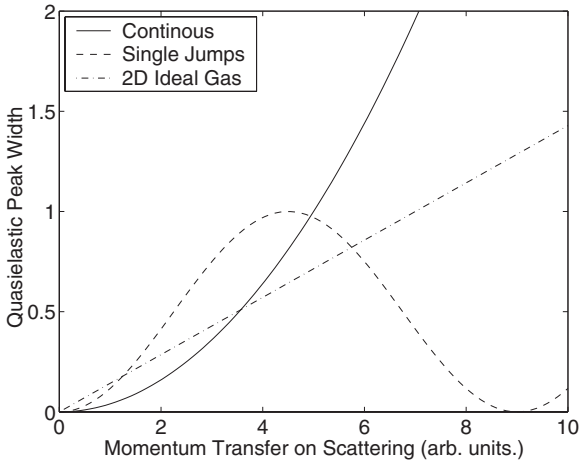

Figure 1. Variation of the quasi-elastic peak width with momentum transfer, $\Delta \boldsymbol{K}$, in an ideal experiment. The solid curve shows continuous diffusion, the dashed curve is for jump diffusion and the dot–dashed curve represents ideal-gas-like diffusion.

We can model the scattering, provided that we know an appropriate form for the correlation function. It is possible to do the calculation analytically for simple idealized cases of diffusion [8–10]. Vineyard showed that the Van Hove correlation function $G(\boldsymbol{R}, t)$ could be expressed in terms of the self-correlation function $G_s(\boldsymbol{R}, t)$. For continuous diffusion (such as Brownian motion), $G_s(\boldsymbol{R}, t)$, when Fourier transformed, gives a Lorentzian QHAS peak shape [8], with a full width at half-maximum (FWHM, ΔE) that has a quadratic dependence on the momentum transfer, $\Delta \boldsymbol{K}$:

$$\Delta E = 2\hbar D \, \Delta K^2 \tag{2}$$

where D is the two-dimensional diffusion coefficient. For jump diffusion, a Lorentzian QHAS peak shape is also produced [10], with a FWHM given by

$$\Delta E = 2\hbar \sum_j \nu_j [1 - \cos(\Delta \boldsymbol{K} \cdot \boldsymbol{j})] \tag{3}$$

where ν_j are the jump frequencies associated with jump vectors $\boldsymbol{j}$. For two-dimensional gas-like diffusion, where the adsorbate runs unimpeded across the surface, Gaussian QHAS broadenings are produced with ΔE being a linear function of $\Delta \boldsymbol{K}$ [13]:

$$\Delta E = 2\hbar \sqrt{\frac{2 \ln(2) k_B T_s}{m}} \, \Delta K. \tag{4}$$

Figure 1 illustrates these results, showing ΔE as a function of $\Delta \boldsymbol{K}$. Real systems are more complex; however, it is evident from figure 1 that observation of the variation of broadening with momentum transfer will give a uniquely detailed picture of the diffusion process. It is important to collect data over a large enough range of momentum transfers to properly cover the reciprocal-space map for the processes involved.

In practice, the quasi-elastic broadening is masked by the resolution of the apparatus. One observes a convolution of the instrumental elastic peak width and the quasi-elastic broadening due to diffusion. The instrumental effect must be separated out in order to analyse the QHAS data, a process which becomes progressively more difficult as the diffusion becomes slower. Given the resolution currently available and that the broadenings under study are usually of

a similar (or smaller) magnitude, it is normally only possible to extract the FWHM of the quasi-elastic peak width, ΔE [14].

As most real systems do not conform to the simple diffusion models outlined above, real experimental results, while more interesting, cannot usually be understood with such ease. In order to perform a rigorous analysis of the data it is normally necessary to use molecular dynamics (MD) simulations to model the motion of the diffusing particles [5, 15] and generate a $G(\boldsymbol{R}, t)$ which in turn can be used to simulate a quasi-elastic peak shape for comparison with the observations.

There are a range of benefits when using the QHAS technique to study diffusion, along with a few limitations. The primary advantage is that, unlike nearly all other techniques, it is capable of monitoring the adparticle motion over the same timescales as that on which normal diffusion occurs. Measurements are taken *in situ*, in real time and are absolutely non-destructive. Thus, realistic equilibrium measurements are possible.

2. Experimental methods

An experiment must be sensitive to the small changes in particle velocity that are characteristic of quasi-elastic scattering. The faster an adsorbate moves on the surface, the greater the energy broadening that arises in the probing atom beam. It follows that the energy resolution of an experiment provides a lower limit to the range of diffusion phenomena that can be studied. Until recently, energy resolution has been the main limitation of the technique and QHAS studies have generally been restricted to systems where the diffusion is exceptionally fast ($D > 5 \times 10^{-6}$ cm^2 s^{-1} [1]). In the drive to extend the range of accessible systems, new methods are being developed and, in the present section, we provide a brief description of the two major techniques.

2.1. The time-of-flight technique

The time-of-flight technique is established as the standard tool for inelastic scattering measurements and has been applied in many QHAS studies [4]. The principle of the method is illustrated schematically in figure 2, where the progress from beam production to detection is represented in a linear manner from left to right. After leaving the source, the beam is modulated by a mechanical chopper before interacting with the sample. Scattered atoms then traverse a fixed distance before reaching the detector, where their time of flight from the chopper is recorded. The quasi-elastic broadening is determined by comparing time-of-flight distributions before and after scattering. The distribution before scattering can be obtained, for example, by observing the specularly scattered beam ($\Delta \boldsymbol{K} = 0$), for which there is no quasi-elastic broadening.

There are two main contributions to the resolution of the experiment. The first is the accuracy of the timing, which depends on factors such as the opening time of the chopper and the uncertainty in the length of the flight path due to the size of the detection region. Second, the distribution of velocities in the incident beam gives rise to an intrinsic uncertainty in the incident velocity and hence to any change in velocity that takes place on scattering. The latter effect, which typically gives an experimental peak broadening of FWHM 0.3 meV under optimum conditions, imposes a fundamental lower limit on the quasi-elastic broadening that can be resolved. The QHAS data reviewed in this paper were obtained with spectrometers that achieve very high count rates, corresponding to typically (if the detector were not to saturate) some 300 MHz to 1 GHz at the specular condition for a well ordered flat metal or ionic crystal surface [4]. With these high signals it is possible to measure relatively small increases in

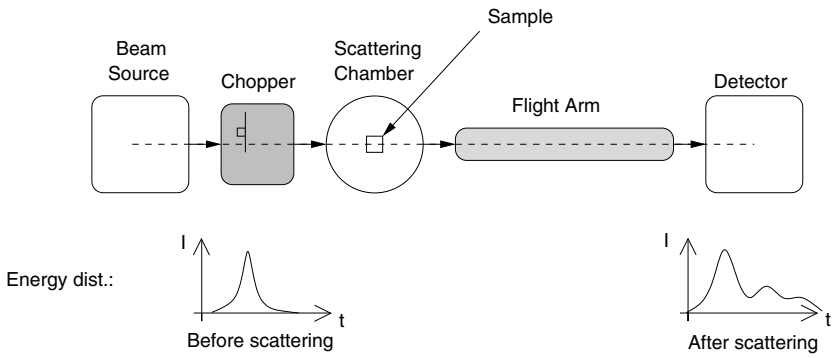

Figure 2. A schematic drawing of a time-of-flight helium scattering apparatus. The experiment is represented in a linear manner, with the helium beam running from left to right. The momentum transfer on scattering, $\Delta \boldsymbol{K}$, is determined by the beam energy and the angle between the source and detector. The sketches of the energy distribution indicate that before scattering the spectrum is given only by the intrinsic properties of the apparatus. After scattering the spectrum contains additional structure due to inelastic interactions with the surface.

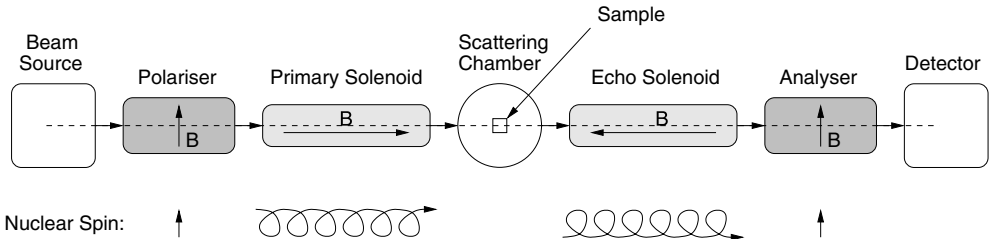

Figure 3. A schematic ^{3}He spin-echo spectrometer for performing QHAS measurements. The ^{3}He beam is polarized in an inhomogeneous magnetic field. The spin is 'wound up' in the primary solenoid, scattered from the sample, 'unwound' in the secondary solenoid and finally spin analysed before detection.

the width of the QHAS peak and extract true QHAS broadenings down to 30 μeV [5, 14]. This achievement represents a detection limit that is unlikely to be bettered without significant advances in the technology for either beam production or beam modulation.

2.2. The spin-echo technique

The spin-echo approach overcomes the main limitation imposed by the velocity distribution in the beam. The technique determines the energy change on scattering using NMR-like spin precession in the nuclei of a helium-3 beam and was first developed in the mid-1990s [7]. When compared with time-of-flight methods, improvements in resolution of nearly four orders of magnitude have been reported [16, 17]. The technique is illustrated schematically in figure 3. The beam progresses, left to right, from source to detector. On the incident leg, between the source and sample, there is a beam polarizer, which aligns the ^{3}He nuclear spins, followed by a spin-precession solenoid. On the outgoing leg, the scattered atoms pass first through a further spin-precession solenoid before entering a spin analyser and detector.

The principle of the method can be understood as follows. The polarizer prepares a plane-polarized beam with the spin direction perpendicular to the axis of propagation. The first spin-precession solenoid has its field aligned along the propagation axis so that, on entry, the

spin of each ^{3}He nucleus undergoes a Larmor precession in the field. The total precession angle of each atom, ϕ, depends on the integral of the axial field calculated along the trajectory. Thus,

$$\phi_1 = \gamma \int B_1(z)\,\mathrm{d}t = \frac{\gamma}{v_1}\int B_1(z)\,\mathrm{d}z, \tag{5}$$

where γ is the gyromagnetic ratio for ^{3}He ($\gamma = 2\pi \times 32.433$ MHz T^{-1}), B_1 is the magnetic field in the solenoid and v_1 is the velocity of the helium atom, which is taken to be in the z-direction. After scattering from the sample, atoms enter the second solenoid where they experience a field aligned anti-parallel to the propagation direction. The spins precess again, but in the opposite direction. If the solenoid fields are identical, the total spin rotation, ϕ, will be given by

$$\phi = \phi_1 + \phi_2 = \gamma\left[\frac{v_2 - v_1}{v_1 v_2}\right]\int B(z)\,\mathrm{d}z, \tag{6}$$

where the subscripts 1 and 2 refer to the primary and echo solenoids respectively. If the atoms scatter perfectly elastically from the surface ($v_1 = v_2$), the original polarization will be recovered. Regaining the polarization is called the 'echo' and the point when $\mathrm{d}\phi/\mathrm{d}v = 0$ is known as the spin-echo point. Note that the spin-echo point is the same for all elastically scattered atoms, regardless of their velocity. Thus, the technique is much less sensitive to the initial velocity distribution than the time-of-flight method.

In an experiment, the macroscopic polarization of the beam is measured at the spin-echo point as a function of the solenoid field strength. Different field strengths correspond to measurements over different timescales. The measured polarization corresponds to the temporal cosine transform of the dynamical structure factor for scattering, or the spatial Fourier transform of the Van Hove correlation function.

There are a number of practical difficulties in the implementation of the helium-3 spin echo, due to the small nuclear moment of ^{3}He. The major difficulty lies in polarizing a beam at a high enough energy to allow sufficient momentum transfer on scattering. Measurements over a range of momentum transfer are necessary in order to produce a comprehensive reciprocal-space map of the diffusion process. Intense, precise, magnetic fields are required, over extended lengths. Recently, we have succeeded in polarizing a ^{3}He beam of energy 8 meV, which has enough momentum to enable complete diffusion measurements [18]. The design is based on a hexapole geometry that focuses the ^{3}He beam as well as acting as a polarizer.

2.3. Interpretation

According to the Van Hove equation (1) the scattered intensity as a function of momentum and energy transfer is given, within the kinematic approximation, by a form factor multiplied by the Fourier transform in space and time of $G(\boldsymbol{R}, t)$. Most of the QHAS data taken so far have been for low coverages of atoms and molecules adsorbed on low-index metal surfaces. For this type of system, the helium atoms may be considered to be scattering from isolated bumps on the surface and the conditions for the Van Hove equation to be valid are satisfied. As the coverage is raised, the scattering cross-sections overlap and multiple scattering between different adsorbates becomes important. These effects were investigated for the diffusion of Na on Cu(001), which has become a paradigm for QHAS studies for which extensive experimental data and a number of theoretical investigations are available [5, 15, 19–24]. Eikonal calculations, which can allow for the overlap of scattering cross-sections, show little deviation from the peak widths derived from the Van Hove equation [25]. Similarly, a crude multiple-scattering calculation has also shown little effect [15].

Given the current limits on experimental resolution and the difficulty in obtaining accurate form factors for atom scattering, it is not possible to use the experimental data to determine $S(\Delta \boldsymbol{K}, \omega)$ directly, with sufficient accuracy for $G(\boldsymbol{R}, t)$ to be obtained by taking a Fourier transform. Even if such direct data inversion were possible, it would still be necessary to interpret the $G(\boldsymbol{R}, t)$ obtained in terms of a particular model of diffusion. For sufficiently small broadenings, the *width* (as opposed to the magnitude) of the quasi-elastic peak is independent of the form factor. The main effort in data interpretation then lies in finding a model and optimizing its parameters, so as to give a $G(\boldsymbol{R}, t)$, and hence a $S(\Delta \boldsymbol{K}, \omega)$, that reproduces the dependence of the quasi-elastic peak width on momentum transfer that has been determined experimentally.

Usually the QHAS broadening is so small that the form factor changes little over the range of energy and momentum transfer present in the QHAS peak. In the case of exceptionally large broadenings, the variation in form factor over the QHAS peak becomes important. In the case of the Xe/Pt(111) system, for which QHAS broadenings of up to 3 meV were observed, the variation of the form factor produced peaks that were clearly asymmetric [13]. It was necessary to divide the experimental peak by an approximate form factor before a true QHAS broadening could be extracted.

The main use of the analytical forms of $S(\Delta \boldsymbol{K}, \omega)$, which can be derived for simple diffusion models, is to assist in the understanding of more realistic ones, for which S is usually derived from a MD simulation. These MD simulations have proved a powerful tool in data analysis, enabling the effective potential surface on which diffusing species move to be determined, the interactions between diffusing adsorbates to be probed and the rate of energy transfer between substrate and adsorbate to be obtained.

2.4. MD simulations

MD simulations can require intensive computational effort. The relatively large-scale combined MD and scattering simulations required for QHAS interpretation would therefore appear to present a significant obstacle to the comprehensive analysis of data obtained using the technique. Fortunately, for many classes of system the simulated surface can be simplified considerably while still reproducing the essential experimental features.

Ideally, a comprehensive simulation including the motion of the substrate atoms would be performed to simulate the diffusion process. Such simulations were applied to the Na/Cu(001) system [22,26]. Here, the substrate was represented by a harmonic lattice with a pairwise Morse potential used to represent the Na–Cu interaction. The parameters of the Morse potential were determined such that the adsorption geometry, adsorbate vibrational frequencies and the QHAS determined activation energy were correctly reproduced. When used in MD simulations, the resulting potential yielded a remarkable agreement, not just with the form of the momentum transfer dependence of the QHAS broadening, indicating a correct model for diffusion, but also with the absolute magnitude of the broadening, showing that the simulations were correctly reproducing the rate of energy transfer between the substrate and diffusing species.

MD simulations of that type are particularly time consuming. In addition, it is often difficult to justify a pairwise interaction between the diffusing species and the substrate atoms. Even in the case of Na on Cu(001) the use of a pairwise Morse potential is questionable, since the adsorbate/substrate potential is clearly determined by interactions with the delocalized substrate electrons. Similar problems arise if substrate exchange processes or other many-body effects are important in the diffusion. For certain systems (such as pre-melting metal surfaces), such effects will almost certainly play an important role. However, much of the QHAS information available to date is for heterogeneous adsorption systems. These systems,

where large displacements of substrate atoms are generally not involved, can be simulated using the Langevin approach. Here, the substrate interaction is replaced with an adiabatic potential energy surface, $V(x, y)$, and energy transfer between the substrate and adsorbate is modelled using a combination of a friction (coefficient η) and Brownian motion-type random forces of a magnitude scaled to give the correct system temperature [5, 13, 15, 20]. For systems in the low-coverage limit, no further interaction potentials are necessary. However, with moderate to high coverages, pair potentials can be added to deal with adsorbate–adsorbate interactions (e.g. [15]). Such simplifications provide a dramatic reduction in computational requirements for QHAS analysis, yet still maintain a realistic treatment of the surface dynamics. As a result, the Langevin method is the method of choice in the interpretation of QHAS data and we limit our further discussion to this technique.

The motion of the ith diffusing species is given by the Langevin-type equation

$$m\ddot{\boldsymbol{r}}_i = -\boldsymbol{\nabla} V(x, y) - \eta m\dot{\boldsymbol{r}}_i + \boldsymbol{\xi}_i(t) + \sum_{j\neq j} \boldsymbol{F}_{ij} \tag{7}$$

where m is the mass of the diffusing species, $\boldsymbol{\xi}_i(t)$ is the random force from the substrate on the ith particle and $\boldsymbol{F}_{ij}$ is the force exerted on the ith particle by the jth particle. The trajectories of the diffusing species are computed by numerically integrating the Langevin equation, $\xi_i(t)$ being included by adding random impulses chosen according to a computationally convenient probability distribution (all distributions being equivalent, according to the central limit theorem, provided the time step is small enough). For each simulation run, the intermediate kinematic scattering function, $A(\Delta\boldsymbol{K}, t)$ is calculated from the motion of the diffusing particles:

$$A(\Delta\boldsymbol{K}, t) = \sum_j \exp[-\mathrm{i}\,\Delta\boldsymbol{K}\cdot\boldsymbol{r}_j], \tag{8}$$

where the summation is over all the diffusing particles in the simulation. $\Delta\boldsymbol{K}$ usually corresponds to scattering along a given lattice direction. Fourier transforming the result in the time domain, multiplying by the complex conjugate and then averaging over many simulation runs gives the quasi-elastic peak shape, $S(\Delta\boldsymbol{K}, \omega)$, which can then be convolved with the experimental resolution. The Lorentzian FWHM of the broadening is extracted from the convolved spectrum, using the same numerical technique as is applied to the experimental data, so a direct comparison between the two is possible. The inter-particle potential, particle–surface potential and friction (η) can then be found by fitting to the experimental data.

3. Existing QHAS studies

Since the first demonstration of the technique in the late 1980s, QHAS has been applied to almost 20 distinct systems. In this section we summarize the published QHAS data. The experimental results are loosely separated into diffusion measurements on (i) simple systems, (ii) systems in which strong inter-adatom interactions have been shown to be important and systems concerning (iii) small and (iv) larger molecules.

3.1. Simple adatom diffusion

3.1.1. Self-diffusion on metals: Pb(110), Ni(110) and Ag(110). The first system to be studied using quasi-elastic helium scattering was the diffusion of Pb atoms on a melting Pb(110) surface [27–29]. The experiment involved heating a clean Pb(110) crystal to a temperature close to its melting point (600.7 K) and carefully examining the changes in the profile of the elastically scattered helium beam. Initial results [27] measured at single $\Delta\boldsymbol{K}$ points along the

$\langle 100\rangle$ direction (at 0.64 Å^{-1}) and along the $\langle 1\bar{1}0\rangle$ direction (0.90 Å^{-1}), at temperatures between 300 and 570 K, demonstrated a quasi-elastic broadening. The effect was attributed to an onset of rapid lead-adatom diffusion, starting 50 K below the bulk melting point. The quasi-elastic peak shape data were fitted with a Lorentzian curve, from which the FWHM was extracted. By assuming the $\Delta\boldsymbol{K}$ dependence for continuous diffusion, diffusion coefficients, D, were obtained. The temperature dependence of D was consistent with an activated mechanism and gave an activation energy, E_a, of 650 ± 200 meV. The measured E_a was intermediate between the values for solid and liquid lead (close to the bulk melting point) and hence was used to infer that diffusion is limited by a 'residual crystalline order at the surface' [27].

Later work extended the measurements to a range of $\Delta\boldsymbol{K}$ values in both the $\langle 001\rangle$ and $\langle 1\bar{1}0\rangle$ directions [28,29], showing the diffusion to be strongly anisotropic. Along the $\langle 001\rangle$ direction, the $\Delta E(\Delta\boldsymbol{K})$ dependence suggested jump diffusion over a distance of 4.94 Å, i.e. between the close-packed rows. In the $\langle 1\bar{1}0\rangle$ direction, the broadening increased rapidly with $\Delta\boldsymbol{K}$ and appeared to oscillate slightly, but is not periodic. Hence, despite a slightly unsatisfactory fit, the best model was concluded to be jump diffusion over a range of continuously distributed lengths, with an average of 4.4 Å.

Graham *et al* [14] have studied diffusion of Ni on Ni(110) in the range 900–1200 K. By measuring the quasi-elastic broadening at 0.43 Å^{-1} they produced an Arrhenius plot to obtain effective activation energies of 536 ± 40 meV and 424 ± 40 meV along the $\langle 1\bar{1}0\rangle$ and $\langle 001\rangle$ directions respectively. The mechanism was studied by measuring over a range of $\Delta\boldsymbol{K}$ from 0 to 3 Å^{-1} along the $\langle 1\bar{1}0\rangle$ direction, at both 1000 and 1100 K. Both sets of results show characteristics of jump behaviour. The model is in exceptional agreement with a simple 80% single-jump/20% double-jump model, suggesting that any vibrational contributions are small and the adatoms remain on a well defined lattice. The fitted model was used to obtain diffusion coefficients in the small-$\Delta\boldsymbol{K}$ (long-length-scale) limit: 2.5×10^{-5} and 5.1×10^{-5} cm^2 s^{-1} at 1000 and 1100 K respectively. They report that these values are in moderate agreement (with a factor of 50%) with mass transport measurements.

A small study has been performed on the self-diffusion of K on ultrathin K layers, supported by a Ni(110) crystal [30]. At temperatures above 250 K the quasi-elastic peak was strongly affected by K desorption, but below this, temperature-activated behaviour was observed. An activation energy of 63 ± 15 meV was extracted from the broadening at 0.3 Å^{-1} (i.e. for motion over 20 Å length scales), but as the micro-scale structure of the K layers was not well defined and multiple domains were present, the activation energy could not be associated with diffusion in a particular lattice direction. The results for the $\Delta E(\Delta\boldsymbol{K})$ curves do not lend themselves to definite conclusions for the diffusion mechanism, despite some suggestions of jump behaviour.

Some preliminary data have been obtained for the self-diffusion of Ag on Ag(110) between 300 and 750 K and for momentum transfers up to $\Delta\boldsymbol{K} \simeq 1$ Å^{-1} (length scales >6 Å) [31]. Little diffusion was detected below 600 K. At higher temperatures a significant quasi-elastic broadening was observed and fitted to a single/double-jump model, giving an activation energy of 190 meV.

3.1.2. S on Cu(111). The first heterogeneous adsorbate system studied using QHAS was S on Cu(111). Hinch *et al* [12] made use of residual traces of sulphur contamination within the bulk of a Cu(111) single crystal. During extended annealing at above 800 K, sulphur was found to segregate from the bulk, providing an S coverage that increased uniformly with time. Measurements were carried out for $\Delta\boldsymbol{K} = 0.0$–$1.0$ Å^{-1} along the $\langle 1\bar{1}0\rangle$ direction, at 820 K only, but for coverages of up to 0.16 ML. The extracted FWHM quasi-elastic broadening as a function of $\Delta\boldsymbol{K}$ showed good agreement with the quadratic form expected for continuous

diffusion, giving a diffusion constant of $D = 2.87 \times 10^{-5}$ cm^2 s^{-1}. Within the coverages measured, the diffusion rate was found to remain constant, i.e. no effects of sulphur–sulphur adatom interactions were detected.

3.1.3. H and D on Pt(111). Graham *et al* [32] have performed a comprehensive study of both H and D on Pt(111). Within the temperature range 140–250 K and over a wide range of coverages (0.05–0.66 ML) they measured the quasi-elastic broadening along the $\langle 11\bar{2}\rangle$ and $\langle 1\bar{1}0\rangle$ directions. The shape of the $\Delta E(\Delta \boldsymbol{K})$ curves strongly suggests a jump mechanism. Analysis was carried out in terms of a simple jump model, based on the jumps that were expected to occur (nearest-neighbour jumps along the 60°-separated lattice directions). The results for a simple single-jump model showed very good agreement with the data.

Arrhenius plots of the quasi-elastic broadening at 0.44 Å^{-1} indicate activated behaviour, giving activation energies of 68 ± 5 meV for H and 76 ± 7 meV for D. The difference was attributed to the difference in zero-point energy between H and D. An analysis of coverage dependence showed a drop in both activation energy and pre-exponential factor with increasing coverage. The drop was attributed to the effect of nearest-neighbour H–H repulsion, which becomes more important with coverage and reduces the effective barrier to jumping. The relatively weak dependence on coverage was taken to indicate that the diffusion is dominated by the effect of the substrate.

3.1.4. Xe on Pt(111). The QHAS measurements of Xe diffusion on Pt(111) [13] are quite unusual. Firstly, Xe atoms diffuse very rapidly and so produce exceptionally large QHAS broadenings: up to about 3 meV. The diffusion mechanism is also unusual. Ellis *et al* [13] chose the conditions to correspond to a 2D gas phase and on measurement they observed an almost completely linear dependence of a Gaussian peak width on momentum transfer (cf the usual Lorentzian shape). The peak shape and $\Delta \boldsymbol{K}$ dependence strongly suggested 2D ideal-gas-like diffusion and, thus, provided the first explicit observation of a 2D ideal gas.

Because the width of the quasi-elastic peak from mobile Xe is so large, it is masked by the elastic peak (from the substrate) and appears only as a 'quasi-elastic foot' [13]. The shape of the foot becomes distinctly asymmetric as the scattering momentum transfer increases. The asymmetry is due to the variation in the scattering form factor over the quasi-elastic peak. Including this factor allowed the Gaussian broadening to be extracted and gave the linear $\Delta E(\Delta \boldsymbol{K})$ dependence.

Langevin MD simulations were used to examine the system in more detail. These used a rigid, corrugated substrate and Xe–Xe inter-adsorbate forces. The linear $\Delta E(\Delta \boldsymbol{K})$ dependence was well reproduced by the simulations. Significant deviations from the measurements were apparent only in simulations with friction, $\eta > 0.25$ ps^{-1} and for a surface corrugation >9.6 meV, giving upper limits for the properties of the system. Ellis and Graham [5] have also published a series of simulations of high-coverage Xe diffusion on a flat substrate to demonstrate the use of QHAS as a probe of correlated motion.

3.2. Strongly interacting adatom diffusion

3.2.1. Na on Cu(001). Alkali metals on close-packed transitional metal surfaces exhibit an extremely high adatom mobility, making them suited to study using QHAS. Na on Cu(001) was the first system on which adatom jump diffusion was observed by means of QHAS [26] and has been characterized in some detail [5,15,19–23]. Initial measurements were carried out at low coverages where sodium adsorbs as isolated adatoms, which interact by dipole–dipole repulsion [21]. A maximum at about 1.8 Å^{-1} in the $\Delta E(\Delta \boldsymbol{K})$ curve strongly suggested

discrete jumps between lattice sites, but the zero broadening predicted by simple analytical jump diffusion models was not seen. An activation energy of 51 ± 1 meV and a jump attempt frequency of 0.53 THz were obtained from the broadening at $\Delta \boldsymbol{K} = 1.7$ Å^{-1} (jumps of about 3.7 Å). A series of MD simulations were applied, using a vibrating-slab model of the surface [22, 26] which showed very good agreement with the experiment data. At small $\Delta \boldsymbol{K}$, the simulations overestimated the broadening, suggesting an overestimation of multiple-site jumps. It was also shown that a combination of the vibrational motion of the atom and the effect of experimental resolution hide the zero broadening expected from simple models.

Further measurements produced a comprehensive data set, at lower coverages (<5%), over a wide range of temperatures (150–390 K) and in multiple lattice directions [19, 21]. A distinct diffusional anisotropy was observed. The data were interpreted with the aid of a Langevin MD simulation. The main conclusions were the production of a detailed empirical potential energy surface for diffusion, which gives a comprehensive description of low-coverage Na/Cu(001) [19]. Using the optimized potential, the simulations show very good agreement with the QHAS data. From the PES, they also calculate the frustrated translation vibration (T-mode) frequency, including a shift and broadening with temperature. These independent T-mode simulations show excellent agreement with the measurements. Interestingly, the optimized potential seems to suggest the presence of small wells on the atop sites. This may simply be an artifact of the functional form used, or may represent real, transient adsorption sites, similar to those seen with K on Cu(111) and Ni(111) [33], which have not yet been observed experimentally. The authors of [19, 21] point out that there is no guarantee that their potential is unique.

It is interesting that the potential barrier (75 meV) is considerably larger than the measured QHAS activation energy (52.9 ± 0.9 meV at 0.86 Å^{-1}), an effect that is often observed using QHAS. Several possible causes were suggested, including the need for low temperatures before true activated behaviour can be seen (e.g. $k_B T \leqslant E_d/3$), vibrational contributions masking the true diffusional activation energy (particularly at large $\Delta \boldsymbol{K}$) and a need to analyse results in the large-distance/small-$\Delta \boldsymbol{K}$ limit. In section 4 of this article we illustrate that the most important factor may be the frictional coupling to the surface, which has a major effect on the QHAS-measured activation energy, independently of the potential barrier.

Most recently, the effect of increasing the sodium coverage up to $\Theta = 0.18$ has been examined [15, 23]. With larger coverages, the forces between neighbouring Na atoms become much more important. Experiments show three main effects as the coverage is increased:

(i) an increase in the activation energy,
(ii) the shape of the $\Delta E(\Delta \boldsymbol{K})$ curve changes and
(iii) the maximum broadening increases.

The importance of the Na–Na interactions means that the higher-coverage data are more difficult to analyse, and MD simulations are essential. The simulations reproduce both the increase in activation energy with coverage and the change in shape of the $\Delta E(\Delta \boldsymbol{K})$ curves, which comes from the repulsive interaction between atoms. The increasingly rapid rise of the $\Delta E(\Delta \boldsymbol{K})$ curve at small values of $\Delta \boldsymbol{K}$ appears to be due to an increasing number of long jumps. However, by calculating both incoherent and coherent scattering (summing intensity versus amplitude), Ellis *et al* [15] showed the form of the $\Delta E(\Delta \boldsymbol{K})$ curve to be due to coherent scattering, originating from increasingly correlated motion of sodium at higher coverages. The origin of the large increase in magnitude of the QE peak width with coverage remains a mystery.

3.2.2. Na on Pt(111). Published work on the low-coverage Na/Pt(111) system has concentrated on the macroscopic diffusion properties that can be extracted from the measure-

ments [34]. Such data can be modelled using Fick's law without the need for MD simulations. The published data were taken for $\Delta \boldsymbol{K} < 0.3$ Å^{-1}, (> about 20 Å or roughly 50 random jumps). The data showed a very good fit to the quadratic $\Delta E(\Delta \boldsymbol{K})$ form expected, allowing diffusion constants to be obtained for a range of temperatures. From the temperature dependence, a very low activation energy of 21.5 ± 1 meV was extracted. A simple comparison with an analytical model of 70% single jumps, 30% double jumps showed rough agreement. More data and more comprehensive analysis will be required to make a full analysis of the mechanism, and MD simulation including Na–Na interactions will almost certainly be necessary.

3.2.3. Ge on Ge(111). QHAS analysis has been used to improve the understanding of Ge-adatom diffusion on Ge(111) [35]. Several techniques (ion scattering, EELS etc) have suggested that above a transition temperature of $T_c = 1050$ K and close to the melting point ($T_m = 1211$ K) the outer layers of Ge are metallic and liquid-like. However, helium-atom diffraction also shows that the surface must remain well ordered. It is known that just below T_c a diffuse signal comes from ∼25% disordered coverage of Ge atoms and the diffuse signal is proportional to the number of adatoms.

A detailed study of the quasi-elastic peak as a function of temperature revealed a decay in height, due to Debye–Waller behaviour, which abruptly stops between 1050 and 1110 K. This was interpreted as due to a uniform and continuous increase in the adatom coverage. The elastic peak remains unbroadened until 1050 K, at which point there is an abrupt onset of broadening, which indicates rapid adatom diffusion. $\Delta E(\Delta \boldsymbol{K})$ curves were measured at 1070 K to examine the diffusion mechanism. In the small-$\Delta \boldsymbol{K}$ limit, the data were used to extract a macroscopic diffusion coefficient, giving $D = (1.2 \pm 0.3) \times 10^{-4}$ cm^2 s^{-1}. The value of D is roughly five orders of magnitude larger than STM diffusion measurements on medium-temperature Ge, but is comparable with the diffusion coefficient of liquid Ge, so is consistent with a highly mobile surface layer. The shape of the $\Delta E(\Delta \boldsymbol{K})$ curves shows a characteristic jump diffusion shape, with flattened peak and well defined minimum (of zero broadening) at the reciprocal-lattice point. The results indicate a strong residual lattice structure, which explains the previous HAS diffraction measurements. The authors conclude by providing a model that can incorporate all the existing experimental results. Essentially, as the temperature of the Ge is increased above 1050 K, more mobile adatoms are produced and the surface corrugation becomes smoother. The effect leads to the much higher, liquid-like diffusion rates seen, although the jumps occur between well defined lattice sites to give the overall ordered structure that is seen with helium diffraction.

3.3. Small molecules

The only small molecule to have been studied comprehensively using QHAS is CO. The technique has been applied to four CO/metal systems; Ni(110), Ni(001), Cu(001) and Pt(111). These measurements push the current resolution of time-of-flight QHAS to the limit. The diffusion of CO is considerably slower than that of the single atoms above, so the quasi-elastic broadening is much smaller and is only just resolvable above the intrinsic resolution and noise of the spectrometers.

3.3.1. CO on Ni(110) and Ni(001). For CO on Ni(110) the quasi-elastic broadening was measured for a coverage of $\Theta = 0.15$ and temperatures in the range 200–360 K [36]. The $\Delta E(\Delta \boldsymbol{K})$ results show qualitatively similar behaviour to that of Na on Cu(001) and have been reasonably well modelled in terms of a Chudley and Elliot jump model (62/38% and 86/14% for single/double jumps along the $\langle 1\bar{1}0 \rangle$ and $\langle 001 \rangle$ directions respectively). As with Na/Cu(001) the main discrepancies are at the reciprocal-lattice points and at low $\Delta \boldsymbol{K}$, due to vibrational

contributions and imperfect (non-instantaneous) jumps. MD simulations will be needed to explain these observations fully and may allow a simple diffusional potential to be developed. The activation energy values obtained are considerably lower than those obtained using other techniques; 57 ± 4 meV along the close-packed rows ($\langle 1\bar{1}0 \rangle$) and 35 ± 4 meV perpendicular to the rows ($\langle 001 \rangle$). An explanation of the lower diffusion barrier across the close-packed rows, contrary to what is intuitively expected, has still not been forthcoming. Measurements for low-coverage CO on Ni(001) also show an activation energy of about 60 meV and for both surfaces of nickel there is relatively little coverage dependence on the activation energy [37].

CO on nickel illustrates a general observation that the QHAS technique often reports lower diffusion barriers than other methods [1]. For example, for H/Pt(111), laser-induced thermal desorption (LITD) gives activation energies of 500 meV, compared to 70 meV obtained using QHAS. The controversy that this effect triggered now seems to have been resolved. It has been established that the QHAS measurements apply to diffusion over atomically flat terraces [32, 34], whereas the higher diffusion barriers, obtained by semi-macroscopic techniques, are the result of the much larger activation energies for diffusion over step edges. The issue was resolved by recent PEEM measurements, which yielded values similar to those from the QHAS technique in step-free regions [34].

3.3.2. CO on Cu(001) and Pt(111). QHAS results obtained for CO on Cu(001) and CO on Pt(111) are much less detailed than for CO on Ni. Resolvable broadenings could only be measured at single $\Delta \boldsymbol{K}$ values. For CO/Cu(001), broadenings at $\Delta \boldsymbol{K} = 3.5$ Å^{-1} were measured between 110 and 150 K, while on CO/Pt(111) at $\Delta \boldsymbol{K} = 1.3$ Å^{-1} only a single measurement at $T = 400$ K could be obtained. Although not comprehensive, the data can still be used to provide some insights and draw together the physical picture of these systems. In the copper case, the derived activation energy ($E_a = 31 \pm 10$ meV) was used to estimate the diffusion barrier height on a simple empirical CO/Cu(001) potential energy surface [6, 38, 39].

For CO on Pt(111), Graham and Toennies [40] assume that the mechanism is purely single-jump diffusion to obtain a jump frequency and diffusion rate. They combine these results with a pre-exponential factor estimated from the T-mode data to suggest an activation energy of 130 ± 20 meV.

3.4. Larger molecules

Few larger molecules have been examined using the QHAS. However, the development of spin-echo QHAS will allow much slower diffusion rates to be measured and so will allow a wider range of systems to be examined.

3.4.1. Hydrocarbons. The diffusion of methane on Pt(111) has been studied at 69 K and a coverage of $\Theta = 0.2$ [41]. Large quasi-elastic broadenings were produced: up to about 3 meV. In this case, the extracted broadening was shown to agree well with simulated results for a quasi-ideal 2D gas, indicating that the surface is exceptionally smooth and the surface friction is low. However, the effective mass, deduced from experiment, is 54 amu, greater than that expected for methane. Ellis has performed a series of simulations which seem to point to clustering as the origin of this effect [41]. Fuhrmann and Wöll have also used QHAS analysis as part of their study of the two-dimensional melting transition of long-chain hydrocarbons on Pt(111) [42]. From an analysis of the quasi-elastic peak shape at 200 K and $\Delta \boldsymbol{K} = 0.52$ Å^{-1}, they conclude that the 160 K transition observed with octane was to a two-dimensional liquid state.

3.4.2. $C_{24}H_{12}$ on Au(111). The only surface system studied so far using spin-echo QHAS is coronene ($C_{24}H_{12}$) on Au(111) [17]. Spin-echo curves were measured over the temperature range between 95 and 437 K, for a range of momentum transfers up to 0.25 Å^{-1} along the $\langle 1\bar{1}0\rangle$ direction (corresponding to diffusion over length scales larger than 25 Å). The resulting energy broadenings (of the order 50 μeV) were examined as a function of $\Delta\boldsymbol{K}$ in order to determine the mechanism. The data do not indicate a mechanism clearly, but allowed discrete jumps of 19 Å to be inferred.

4. Application of principles: diffusion of CO on Cu(001)

A number of issues emerge from the review given above, which we illustrate with a case study using data, calculations and simulations for CO diffusion on Cu(001). The system has been studied experimentally and a potential energy curve along the diffusion coordinate has been proposed [6, 38]. The system has also been studied using total-energy density-functional calculations, which suggest a very different form for the potential energy curve [43, 44]. The difference between the experiment and the calculation is significant and requires explanation. As we will show, an explanation can be achieved from an analysis of MD simulations [45]. The work demonstrates that there is no simple relationship between activation barriers obtained from experiment at a particular $\Delta\boldsymbol{K}$ and the adiabatic potential energy barrier.

The potential energy curve derived from experiment is based on measurements of the quasi-elastic broadening at a particular $\Delta\boldsymbol{K}$ value (3.5 Å^{-1} along the $\langle 100\rangle$ azimuth) and for several temperatures between 110 and 160 K [38]. An Arrhenius plot of the quasi-elastic peak width gave an activation energy of 31 ± 10 meV. To obtain an potential energy curve, Graham *et al* then used the frequency of the frustrated translation vibrational mode of CO to give the curvature of the potential around the adsorption sites. When this was taken together with their experimentally derived activation barrier, it was possible to make a simple extrapolation and construct a potential between adsorption sites. Their procedure gave a potential whose important features are a single adsorption site in the unit cell, separated from adjacent sites by a sinusoidal barrier, of approximately 30 meV.

The potential derived from theory is quite different. Ge and King [43,44] used total-energy density-functional calculation to calculate the adsorption energy for a 2×2 CO adlayer on Cu(001) as a function of the lateral registration between adlayer and substrate. Their results are shown as the data points in figure 4 and the line is our interpolation, described later. It is evident from the figure that major differences exist between the calculated potential and the one derived from experiment. First, there are two adsorption sites in the calculated potential, corresponding respectively to on-top and bridge sites. Second, the main barrier to diffusion is approximately 70 meV, more than double the value suggested by experiment.

In the remainder of this section, we explore these apparent conflicts using MD simulations. We reach important, general conclusions in relation both to the interpretation of experimental data, and in relation to the effect of frictional coupling in reducing the apparent activation energy from the value given by an adiabatic potential energy curve. The first stage is to investigate the experimental potential. We have constructed a 2D potential energy surface that is consistent with the form suggested by Graham *et al* [6, 38]. The potential is based on that used previously for Na/Cu(001):

$$V(x, y) = \frac{E_h}{4} + \frac{E_b}{2} + \frac{E_h}{4}\left[\cos\left(\frac{2\pi x}{a}\right) + \cos\left(\frac{2\pi y}{a}\right)\right] + \frac{1}{4}(E_h - 2E_b)\cos\left(\frac{2\pi x}{a}\right)\cos\left(\frac{2\pi y}{a}\right). \tag{9}$$

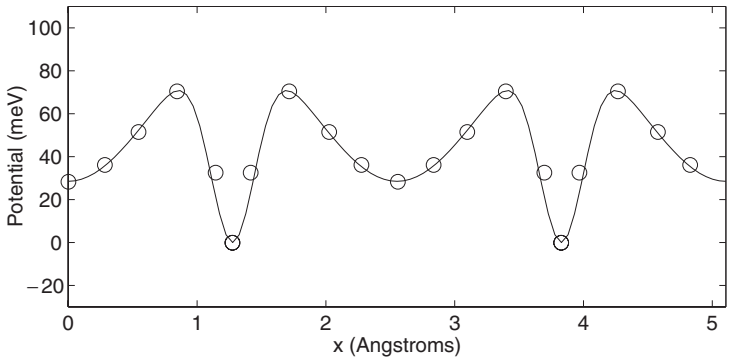

Figure 4. The calculated potential energy surface for diffusion of CO on Cu(001) as calculated by Ge and King [44]. The calculations are shown as open circles and the solid curve is the interpolation used for the MD simulations, as described in the text.

E_b represents the bridge-site barrier and E_h the energy at the adsorption site. These energies give the two parameters that may be varied. In the simulations, the frictional coupling between the CO molecule and substrate ($\eta = 0.125$ ps^{-1}) was taken from the lifetime of the frustrated translation vibrational mode ($\tau = 1/\eta = 8\pm1$ ps) [46]. Simulations of the motion of an isolated CO molecule, as indicated in section 2.4, enable the whole experimental process, including the Arrhenius analysis of quasi-elastic broadening, to be modelled. The free parameters in the potential were varied until the experimental results were reproduced. Applying this process, we found that $E_b = 45 \pm 10$ meV and $E_h = E_b + 5(\pm5)$ meV gave the best agreement with the experimental measurements. Thus, the simulation indicates that a simple Arrhenius type of analysis using data at a single $\Delta\boldsymbol{K}$ underestimates the adiabatic barrier by a significant and unknown margin. Our result is consistent with the view that QHAS measurements consistently underestimate diffusion barriers [43]; however, the underestimation arises not from the experiment itself, but from the approach that has been taken to data analysis in the past. The importance of MD simulations in generating a correct interpretation of data is self-evident.

We now turn to diffusion using the potential calculated by Ge and King [43, 44]. As before, a 2D potential energy surface must be constructed from the existing results in a way that is consistent with the symmetry of the system. We have chosen the following form to extrapolate from the calculated data points [44, 47]:

$$
\begin{aligned}
&V = V_1 + V_2 + V_3,\\
&V_1 = \frac{1}{2}(E_f - E_t)\left[\sin\left(\frac{2\pi x}{a} - \frac{\pi}{2}\right)\sin\left(\frac{2\pi y}{a} + \frac{\pi}{2}\right) + 1\right] + E_t,\\
&V_2 = -(E_f - E_b)\left[\sin^{\alpha}\left(\frac{\pi x}{a}\right)\sin^{\beta}\left(\frac{\pi y}{a} - \frac{\pi}{2}\right) + \sin^{\beta}\left(\frac{\pi x}{a} - \frac{\pi}{2}\right)\sin^{\alpha}\left(\frac{\pi y}{a}\right)\right],\\
&V_3 = (E_h - E_t)\left[\sin^{\gamma}\left(\frac{\pi x}{a}\right)\sin^{\gamma}\left(\frac{\pi y}{a}\right)\right],
\end{aligned}
\tag{10}
$$

where the parameters $E_b = 70.0$ meV, $E_t = 28.5$ meV and $E_h = 85.5$ meV are chosen to match the measured properties of the potential (bridge energy, top-site energy and hollow-site energy). The parameters $E_f = 90$ meV, $\alpha = 22$, $\beta = 12$ and $\gamma = 4$ are adjusted to fit the double-well shape of the data. The resulting fit is shown as the solid curve in figure 4, where it is evident that all the main features of the potential are reproduced. Our results are independent of the choice of the exact form of the potential function.

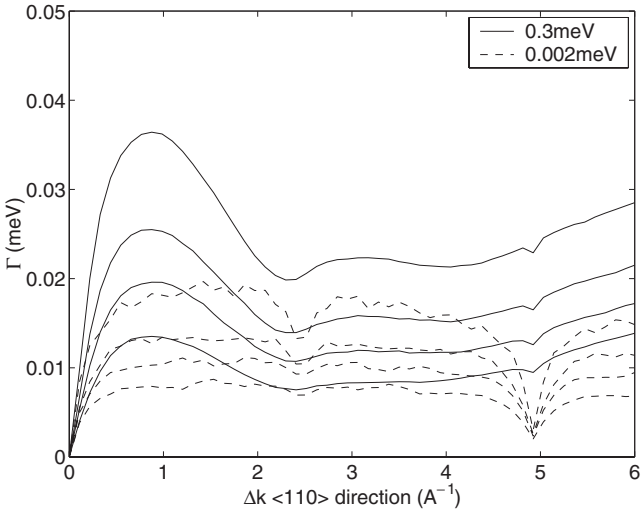

Figure 5. Simulated quasi-elastic broadening along ⟨110⟩ (de-convoluted FWHM Lorentzian peak width) for CO diffusion over Cu(001) using our interpolation of the Ge and King first-principles potential. Curves are shown, giving increasing broadening, at temperatures of 114, 125, 135 and 150 K. The solid curves are for an experimental resolution of 0.3 meV and the dashed curves correspond to 0.002 meV.

Simulations on this potential with the same frictional coupling as before have been used to determine the experimental quasi-elastic broadening as a function of temperature for two different experimental regimes. In the first regime, we assume an experimental resolution of 0.3 meV, like that in the time-of-flight measurements of Graham *et al* [38]. For the purposes of comparison, the second regime is chosen to have a resolution corresponding to 0.002 meV, which could realistically be achieved using spin-echo methods. The results therefore reflect the sensitivity of experiment to factors such as the ability to resolve jumps between the different adsorption sites and show the conditions under which the signature for such behaviour might be evident.

Figure 5 shows the calculated quasi-elastic broadening in the ⟨110⟩ direction for a range of surface temperatures. The full curve corresponds to the time-of-flight experiment and the dotted curves would be obtained with the higher resolution. The two sets of curves are qualitatively different and only the high-resolution data give a true picture of the diffusion processes. For example, the distinct minimum in the dashed curves observed near 4.9 Å^{-1} indicates that the predominant diffusion mechanism is jumping between on-top and bridge sites, i.e. over a length scale of $2\pi/4.9$ Å^{-1} = 1.28 Å. At higher temperatures, a second dip develops near 2.45 Å^{-1} indicating an increase in the number of double jumps from bridge to bridge site, or on-top to on-top site, i.e. between the same well types in adjacent unit cells. None of this behaviour would be evident from a simple inspection of the lower-resolution data. The results demonstrate that the experimental resolution affects the measured broadening in a complex way. The diffusion mechanism is only evident from a simple analysis of the data when the experimental resolution is sufficiently high and when the mechanism is sufficiently simple that it can be compared to a known model. These are strong arguments for seeking improvements in the experiment of the type offered by the spin-echo method.

The results in figure 5 reinforce the argument for a full analysis of the data using MD simulations; however, they do not address the question of how well the Ge and King potential

Table 1. QHAS experimentally determined activation energies and pre-exponential factors (top row), compared with the results of simulation using the first-principles potential. The simulations (rows 2 and 3) use different values of the frictional coupling to the surface, close to the experimental value of $\tau = 8 \pm 1$ ps. All the results correspond to the $\langle 100 \rangle$ direction and a resolution of 0.3 meV.

	E_{act} (meV)	Γ_0 (μeV)
Experiment	31 ± 10	1100 ± 400
Simulation ($\tau = 8$ ps)	38	520
Simulation ($\tau = 6$ ps)	41	810

matches the existing experimental data. In order to answer this final question we have calculated the 'experimental' diffusion barrier for the Ge and King potential. By this we mean the barrier height that would be obtained for diffusion on the Ge and King potential, given the same analysis of the experiment as that employed by Graham and Toennies. The key results are shown in table 1, where activation barriers and pre-exponential factors from two simulations are compared with experiment. The two simulations use different a frictional coupling near to the value indicated in an independent experiment [46]. Reducing the frictional coupling leads to a bigger 'experimental' activation energy and larger pre-exponential factor, showing that the parameter is important in controlling the nature of the diffusion. The important conclusion from table 1 is that the Ge and King calculation is not at odds with the experimental data. However, only measurements performed with significantly improved experimental resolution would allow a critical evaluation of their calculated potential.

5. Conclusions

Since the first QHAS results were published in 1988, a wide range of systems have been studied. The technique has been shown to be a powerful probe, in both reciprocal space and time, of the details of diffusion on atomic scales of length and time. The QHAS technique enables the motion of species on a surface to be monitored continuously, on a truly picosecond timescale.

Whilst simple analytical models exist for the interpretation of the data, MD simulations are needed to access the wealth of information provided by the technique and to relate a particular diffusion model to the observed quasi-elastic broadening. In particular, and with the assistance of MD simulations for the CO/Cu(001) system, we have illustrated the fact that whilst it is tempting to extract 'activation energies' directly from Arrhenius-type plots of quasi-elastic broadenings, the broadening is determined not just by the rate of diffusion, but also by the details of the diffusion mechanism and the resolution with which the measurements are performed. A more careful analysis is needed to give reliable information on the heights of adiabatic potential barriers.

In addition to testing specific potential barrier heights, MD simulations can be used to evaluate the full, two-dimensional potential energy surfaces and also determine the rate of energy transfer between substrate and adsorbate, which is parametrized by the friction parameter η. Contrary to the results of transition state theory [48], in which pre-exponential factors can be deduced from the vibrational frequencies of the adsorbate in the ground and transition states, the QHAS results clearly demonstrate that, as first suggested by Kramers in 1940 [49], the pre-exponential factor and indeed many of the details of the diffusion mechanism are controlled by the friction parameter. The fact that the HAS technique is uniquely capable of yielding simultaneously detailed information on surface diffusion, adsorbate ordering and vibrational frequencies has enabled QHAS to provide one of the few direct experimental evaluations of the transition state theory and Kramers models of surface diffusion [26].

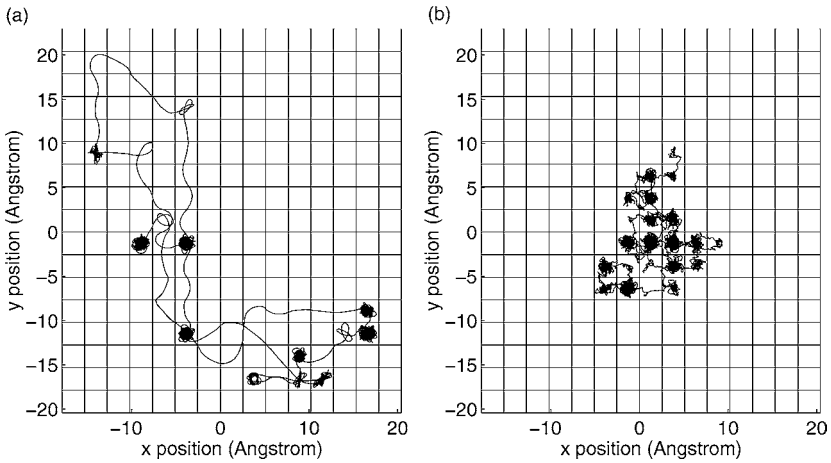

Figure 6. Simulated MD trajectories for (a) low-friction ($\tau = 10$ ps) and (b) high-friction ($\tau = 0.1$ ps) regimes. The simulations are for a sinusoidally corrugated surface with a bridge-site barrier of 45 meV, an atop-site barrier of 50 meV and a temperature of 130 K. The two simulations were run for the same length of time.

The central role of the friction parameter is illustrated in figure 6, which compares MD trajectories for low- and high-friction systems, using the same potential. The motion of the adatom is characterized by vibration about a lattice site, interspersed with jumps between lattice sites. Increasing the friction increases the number of lattice sites visited within the simulation time interval. This is because increasing η corresponds to a rise in the rate at which the diffusing atom changes its energy, which increases both the attempt and success rates for jumps from one site to another. Increasing the friction also reduces the number of multiple jumps as the adatom can no longer 'rollercoaster' across many potential wells before its energy is relaxed back to a bound state. Similar effects have been demonstrated by Chen *et al* [50]. The values of η derived from MD simulations of QHAS data are found to be almost exactly the same as the friction parameter derived independently from the linewidths of adsorbate vibrational modes. Such agreement demonstrates that η does indeed represents a real physical process, as opposed to simply a fitting parameter in MD simulations.

The main limitation on the QHAS technique has been due to the energy resolution of the time-of-flight method, which has meant that only processes occurring on timescales shorter than 0.2 ns can be detected. It has already been shown, however, that the spin-echo technique can extend this range up to around 0.5 μs, which will widen enormously the scope of application of this powerful technique.

References

[1] Barth J V 2000 *Surf. Sci. Rep.* **40** 75–149
[2] Farias D and Rieder K H 1998 *Rep. Prog. Phys.* **61** 1575–664
[3] Comsa G 1994 *Surf. Sci.* **299/300** 77–91
[4] Toennies J P 1993 *J. Phys.: Condens. Matter* **5** A25–40
[5] Ellis J and Graham A P 1997 *Surf. Sci.* **377–379** 833–42
[6] Graham A P and Toennies J P 1999 *Surf. Sci.* **427–428** 1–10
[7] DeKieviet M, Dubbers D, Schmidt C, Scholz D and Spinola U 1995 *Phys. Rev. Lett.* **75** 1919–22
[8] Van Hove L 1954 *Phys. Rev.* **95** 249–62
[9] Vineyard G H 1958 *Phys. Rev.* **110** 999–1010

[10] Chudley C T and Elliot R J 1961 *Proc. Phys. Soc. Lond.* **77** 353–61
[11] Levi A C, Spadacini R and Tommei G E 1982 *Surf. Sci.* **121** 504–18
[12] Hinch B J, Frenken J W M, Zhang G and Toennies J P 1991 *Surf. Sci.* **259** 288–300
[13] Ellis J, Graham A P and Toennies J P 1999 *Phys. Rev. Lett.* **82** 5072–5
[14] Graham A P, Silvestri W and Toennies J P 1997 *Surface Diffusion, Atomistic and Collective Processes* ed M C Tringides (New York: Plenum) pp 565–80
[15] Ellis J, Graham A P, Hofmann F and Toennies J P 2001 *Phys. Rev.* B **63** 195408
[16] DeKieviet M, Dubbers D, Klein M, Schmidt Ch and Skrzipczyk M 1997 *Surf. Sci.* **377–9** 1112–17
[17] DeKieviet M, Dubbers D, Hafner S and Lang F 2001 *Atomic and Molecular Beams: the State of the Art* ed R Campargue (Berlin: Springer) pp 161–74
[18] Jardine A P, Fouquet P, Ellis J and Allison W 2001 *Rev. Sci. Instrum.* **72** 3834–41
[19] Graham A P, Hofmann F, Toennies J P, Chen L Y and Ying S C 1997 *Phys. Rev. Lett.* **78** 3900–3
[20] Chen L Y and Ying S C 1993 *Phys. Rev. Lett.* **71** 4361–4
[21] Graham A P, Hofmann F, Toennies J P, Chen L Y and Ying S C 1997 *Phys. Rev.* B **56** 10 567–78
[22] Ellis J and Toennies J P 1994 *Surf. Sci.* **317** 99–108
[23] Cucchetti A and Ying S C 1999 *Phys. Rev.* B **60** 11 110
[24] Guantes R, Vega J L and Miret-Artes S 2001 *Phys. Rev.* B **64** 5415
[25] Ellis J, unpublished
[26] Ellis J and Toennies J P 1993 *Phys. Rev. Lett.* **70** 2118–21
[27] Frenken J W M, Toennies J P and Wöll Ch 1988 *Phys. Rev. Lett.* **60** 1727–30
[28] Frenken J W M, Hinch B J and Toennies J P 1989 *Surf. Sci.* **211/212** 21–30
[29] Frenken J W M, Hinch B J, Toennies J P and Wöll Ch 1990 *Phys. Rev.* B **41** 938–46
[30] Fuhrmann D and Hulpke E 1997 *J. Chem. Phys.* **106** 3407–11
[31] Pedemonte L, Tatarek R, Vladiskovic M and Bracco G 2001 *20th European Conf. on Surface Science* abstract and talk
[32] Graham A P, Menzel A and Toennies J P 1999 *J. Chem. Phys.* **111** 1676–85
[33] Hofmann F and Toennies J P 1996 *Chem. Rev.* **96** 1307–26
[34] Graham A P and Toennies J P 2001 *J. Phys. Chem.* B **105** 4003–9
[35] Glebov A L, Toennies J P and Vollmer S 1999 *Phys. Rev. Lett.* **82** 3300–3
[36] Bertino M F, Hofmann F, Steinhögl W and Toennies J P 1996 *J. Chem. Phys.* **105** 11 297–304
[37] Hofmann F, Schöllkopf W and Toennies J P 1994 *Proc. Welsh Foundation Conf. on Chemical Research*
[38] Graham A P, Hofmann F, Toennies J P, Williams G P, Hirschmugl C J and Ellis J 1998 *J. Chem. Phys.* **108** 7825–34
[39] Graham A P and Toennies J P 2001 *J. Chem. Phys.* **114** 1051–2
[40] Graham A P and Toennies J P 1998 *Europhys. Lett.* **42** 449–54
[41] Ellis J 1999 *18th European Conf. on Surface Science (Vienna)* oral presentation
[42] Fuhrmann D and Wöll Ch 1997 *Surf. Sci.* **377–9** 544–50
[43] Ge Q and King D A 1999 *J. Chem. Phys.* **111** 9461–4
[44] Ge Q and King D A 2001 *J. Chem. Phys.* **114** 1053–4
[45] Jardine A P, Ellis J and Allison W 2002 at press
[46] Graham A, Hofmann F and Toennies J P 1996 *J. Chem. Phys.* **104** 5311–16
[47] Ge Q, private communication
[48] Hill T L 1960 *An Introduction to Statistical Thermodynamics* (New York: Addison-Wesley) p 198
[49] Kramers H A 1940 *Physica* **7** 284–304
[50] Chen L Y, Baldan M R and Ying S C 1996 *Phys. Rev.* B **54** 8856–61